

# AUTOMATED MAP-MRF EM LABELLING FOR VOLUME DETERMINATION IN PET

Hugh Gribben<sup>1</sup>, Paul Miller<sup>1</sup>, Hongbin Wang<sup>1</sup>, Kathryn Carson<sup>2</sup>, Alan Hounsell<sup>2</sup> and Ashraf Zatari<sup>2</sup>

<sup>1</sup>The Institute of Electronics, Communications and Information Technology (ECIT)  
Queen's University Belfast, Belfast, UK. BT3 9DT

<sup>2</sup>Medical Physics Agency, NI Cancer Centre, Belfast, UK. BT9 7AB

## ABSTRACT

An automated, unsupervised Maximum a Posterior – Markov Random Field Expectation Maximisation (MAP-MRF EM) Labelling technique, based upon a Bayesian framework, for volume of interest (VOI) determination in Positron Emission Tomography (PET) imagery is proposed. The segmentation technique incorporates MAP-MRF modelling into a mixture modelling approach using the EM algorithm, to consider both the structural and statistical nature of the data. The performance of the algorithm has been assessed on a set of PET phantom data. Investigations revealed improvements over a simple statistical approach using the EM algorithm, and improvements over a MAP-MRF approach, using the output from the EM algorithm as an initial estimate. Improvement is also shown over a standard semi-automated thresholding method, and an automated Fuzzy Hidden Markov Chain (FHMC) approach; particularly for smaller object volume determination, as the FHMC method loses some spatial correlation. A deblurring pre-processing stage was also found to provide improved results.

*Index Terms*— MAP-MRF, EM, PET, segmentation

## 1. INTRODUCTION

In this work we aim to evaluate the application of a MAP-MRF EM labelling technique to lesion VOI determination in PET data. This is a subject of vital importance within the area of oncology applications such as therapy evaluation and treatment planning. The traditional approach is semi-automated thresholding, which has been shown to return variable results [1]. Other methods such as clustering and watersheds have been shown to be sensitive to variations in noise intensity and lesion contrast; and also often involve user-dependent initializations [2]. A recent work has used a FHMC approach, due to its unsupervised nature and relatively short computation times [2]. Using this approach, a 3D image is transformed into a 1D chain using the Hilbert-Peano path. Encouraging results were found compared to previous methods. With smaller lesions,

however, it was found that the spatial correlation of such small objects may be lost due to the transformation required. As no such transformation is required with the MAP-MRF EM technique; we hope to be able to overcome this.

## 2. OBSERVATION MODEL

We consider the observation  $Y$  to be a transformed and degraded version of the MRF realization  $X$ , given by

$$Y = B(X) + \varepsilon_i \quad (1)$$

where  $B(X)$  is a blurring effect caused by the imaging system point spread function (PSF), and  $\varepsilon_i$  is independent additive Gaussian noise.

With this model, we need a pre-processing step to compensate for the blurring effect, before segmentation implements the de-noising. For this, we use the Lucy-Richardson deconvolution method [3], which is based upon Bayesian principles. In practice, the PSF is difficult to measure and varies over the field of view. We assume it to be known and constant, so we can model the acquired (blurred) image as a convolution of the ideal image with the camera PSF. For PET images, it can be assumed that the PSF is well approximated by a Gaussian kernel, with a Full Width at Half Maximum (FWHM) of 6mm along the 3 axes for images [4].

For de-noising, a parameter estimation step is essential to our model. For this, we use a mixture modelling approach. We assume each dataset can be modeled by a mixture density of Gaussian distributions. The algorithm used in practice to find the mixture of distributions that best model the dataset is the EM algorithm, first introduced by Dempster et al. [5]. This is an iterative algorithm, which estimates the parameters via a Maximum Likelihood (ML) criterion. The mixture density returned can then be used to associate pixel observations with a Gaussian density in the mixture model, using a simple ML estimation.

To provide a more robust segmentation, however, we integrate into the EM algorithm a MAP-MRF approach.

Using Bayes estimation, the posterior probability of a labelling estimate  $X$  given an observation  $Y$  can be computed by  $P(X|Y) = P(Y|X)P(X)/P(Y)$ , which for a fixed  $Y$  gives us a MAP estimate of

$$X^* = \arg \max_X \{P(Y|X)P(X)\} \quad (2)$$

In MAP-MRF labeling,  $P(X|Y)$  is the posterior distribution of a MRF. The prior model  $P(X)$  takes into account spatial correlations present in an image, and is dependent upon the type of scene. Assuming our scene to be a piecewise constant surface, we consider an indicator function,  $I(X_i, X_j) = 1$  if  $X_i = X_j$  and otherwise  $= 0$ . The Potts model can be described by  $P(X) \propto \exp(\phi \sum_{i,j} I(X_i, X_j))$ , where the sum is computed over all neighbour pairs. Spatial homogeneity in the model is expressed using the parameter  $\phi$ , small values implying randomness, and large values implying uniformity [6]. Let  $N(X_i)$  be the neighbourhood of  $X_i$ , and let  $U(N(X_i), k)$  be the number of neighbourhood voxels with a label corresponding to a distribution  $k$ . The prior energy for each distribution labelled  $k$  can then be defined as the negative of the sum of all the clique potentials over  $X$  [6]

$$E(X) = -\sum_{i \in S} \phi U(N(X_i), k) \quad (3)$$

where  $S$  is the set of voxel sites, and  $i$  the site currently under consideration.

The likelihood model  $P(Y|X)$  depends upon physical considerations.  $Y$  can be assumed to be a degraded version of a MRF realization  $X$  due to independent additive Gaussian noise. Taking a Gaussian distribution as a special form of a Gibbs distribution, advantage is then taken of a MRF's equivalence to a Gibbs's distribution [6], to then define the likelihood as  $P(Y|X) = \exp(-E(Y|X)) / \prod_{i \in S} \sqrt{2\pi\sigma_i^2}$ , where  $\sigma_i^2$  is the variance of the estimated Gaussian distribution at voxel  $i$ , and

$$E(Y|X) = \sum_{i \in S} (X_i - Y_i)^2 / 2\sigma_i^2 \quad (4)$$

is the likelihood energy.

Finally, the prior and likelihood energies are added to yield the posterior energy. This gives

$$E(X|Y) = \sum_{i \in S} (X_i - Y_i)^2 / 2\sigma_i^2 - \sum_{i \in S} \phi U(N(X_i), k) \quad (5)$$

The MAP estimate can then be found by minimising the posterior energy. Practically, this can be performed by the use of the Iterated Conditional Modes (ICM) algorithm, originally introduced by Besag [7]. This is an iterative algorithm that begins with the observed scene  $Y$ , and an initial estimate of the true scene  $X$ . By considering each

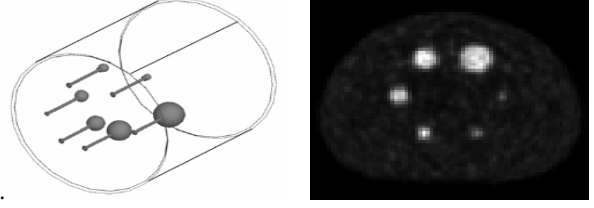


Fig. 1: (a) Graphical Representation of Phantom Object (b) Cross-section of Central Slice obtained from Phantom

voxel site in turn, it then proceeds to provide a new estimate of the true scene iteratively, until convergence is reached, or a maximum number of iterations complete. A single iteration of the ICM requires (6) for each voxel  $i$ , where  $\mu_{k_G}$  is the Gaussian mean of state  $k$ .

$$k^* = \arg \min_k (\mu_{k_G} - Y_i)^2 / 2\sigma^2 - \phi U(N(X_i), k) \quad (6)$$

A label  $X_i$  is then given to voxel  $i$  in the updated estimate  $X$ , corresponding to  $k^*$ . With a traditional method an initial estimate is obtained from the EM Model. Here, however, we fully integrate the ICM algorithm into the EM algorithm, so that for each iteration we have a new estimate, and an optimal parameter estimation using a MAP, as opposed to a ML approach, for the following iteration. The optimal value of  $\phi$  for each iteration is chosen via Pseudo-Likelihood Information Criterion (PLIC) analysis. This is an automated Bayesian technique that considers the ratio of likelihoods of output models to determine the optimal model.

#### 4. RESULTS AND ANALYSIS

The phantom data obtained consists of an oval shaped object containing six fillable spheres of variable diameters filled with fluoro-deoxy-glucose (FDG). The volumes of the spheres range from 0.52 to 26.52 cm<sup>3</sup>. The imagery is 16-bit with dimension 128\*128\*35. Voxels are of size 4x4x4mm<sup>3</sup>, and the signal to background ratio in the imagery is 9:1 with an <sup>18</sup>F-FDG concentration of 17.8kBq/ml in the spheres. A representation of the phantom object and data obtained is shown in Fig. 1.

Each lesion/sphere in the 3D dataset was isolated in a box of similar size (16x16x16 voxels) prior to the implementation of the segmentation techniques. Using prior knowledge of the dataset, it was assumed that each 3D box contained 2 distributions (associated with the sphere of interest and background). The traditional semi-automated thresholding (thresholding with a value of 42% of the maximum intensity value in the lesion based on previous publications [8], referred to as T42) was initially performed, followed by ML EM segmentation, and a non-integrated MAP-MRF segmentation using the output from EM segmentation as an initial estimate. Results showing volume error compared to the true volume for these techniques are

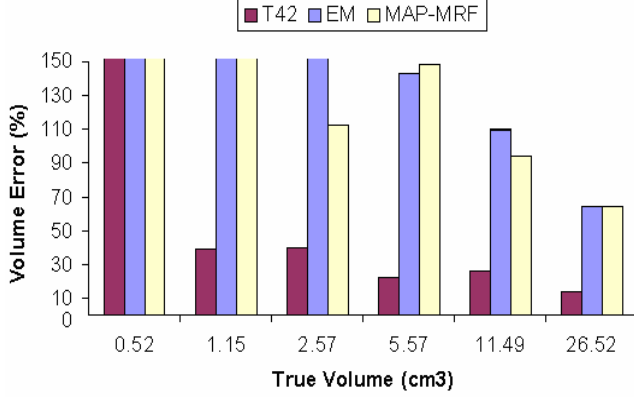


Fig. 2: Volume of Interest errors for T42, EM Model and MAP-MRF Models

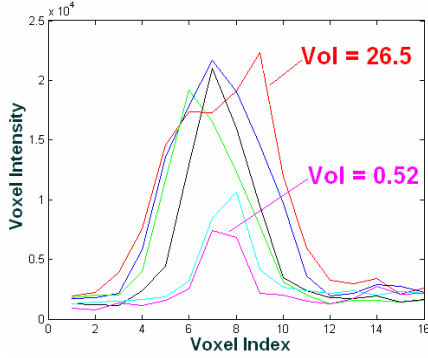


Figure 3: Line Plot of voxel intensity variation along line through the centre of each isolated box of dimension 16x16x16 (Volume of Sphere decreases as half-width of plot decreases)

shown in Fig 2.

Fig. 3 allows us to investigate how the voxel intensities vary for each sphere, and how this contrasts with the background pixel intensities. We can see that for the 2 smallest spheres, the difference between the highest voxel intensity and voxel intensities of the background distribution is much less than for the larger spheres, causing over-estimation in these 2 cases, as the 42% threshold includes voxels that should be classified as background. In the case of the larger spheres, under-estimation occurs due to the larger highest voxel intensities. Here, the 42% threshold excludes voxels that should be classified as belonging to the VOI.

Fig. 2 shows a trend, that as the true volumes of the spheres increase, accuracy in VOI determination increases, with a few exceptions, for all 3 techniques. As the sphere sizes increase, there is smaller overlap in the 2 distributions present in each case, as shown in Fig. 4. In the case of the EM segmentation, this leads to smaller over-estimation of the VOI, as the true volumes increase. This is illustrated in Figs 5(b) and 5(e). Over-estimation, however, still occurs with the larger volumes due to the partial volume effect (PVE) caused by the low resolution of the images.

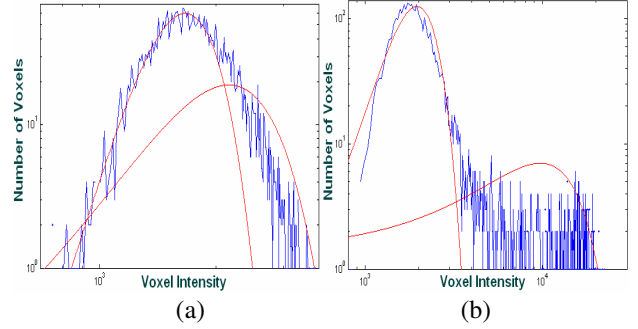


Fig. 4: Gaussian distribution plots obtained via Mixture Modelling shown over the original histogram for spheres of true volume (a) 0.52 (b) 1.15 (c) 26.52 [Log Scale on both x and y-axes]

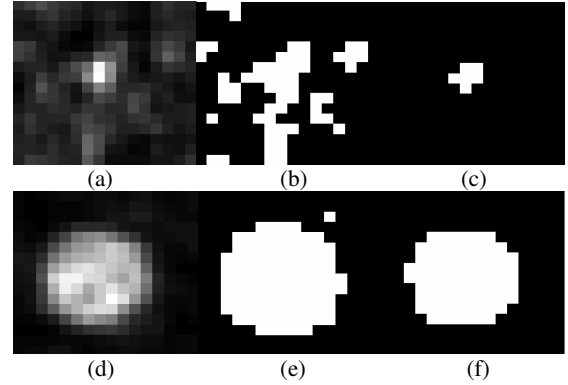


Fig. 5: Centre slice taken from Sphere of Volume = 0.52 (a) Original 16x16x16 Dataset (b) Centre slice from EM Segmentation (c) Output from MAP-MRF EM Segmentation. Centre slice taken from Sphere of Volume = 26.52 (d) Original 16x16x16 Dataset (e) Centre slice from EM Segmentation (f) Output from MAP-MRF EM Segmentation

This can be clearly seen, comparing Figs. 5(d) and 5(e). We see that the pixels on the periphery of the VOI in 5(d) (including elements of both the VOI and background due to PVE) are included in the EM segmentation shown in 5(e).

The MAP-MRF technique provides improvement over the EM result for 4 of the spheres. The results, however, do not match those received using the T42 technique. For the larger spheres, little or no improvement is seen. For this, we can consider the fact that for a pixel situated near the edge of a sphere, after an initial classification there are naturally a higher number of neighbouring pixels classified as belonging to the sphere for larger spheres than smaller spheres. This can be illustrated by considering a pixel at the edge of the VOIs shown in Figs. 5(c) and 5(f). This has the effect of increasing the influence of the 2<sup>nd</sup> term  $\phi U(N(X_i), k)$  in (6) for the component  $k$  relating to the VOI for larger spheres. It is natural; therefore, that the larger the VOI initially, the less likely it would be for the MRF modelling to decrease the volume. For smaller spheres the opposite effect is true, so although the initial

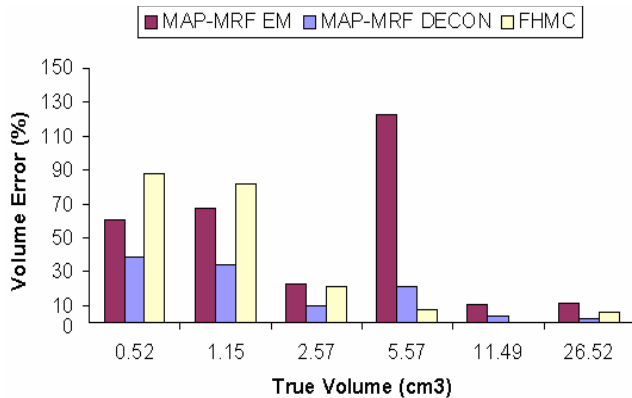


Fig. 6: Volume of Interest errors for MAP-MRF EM, MAP-MRF EM with deconvolution, and FHMC Models (**Note: No Value is available for FHMC for Sphere of Volume 11.49**)

segmentation may not be as accurate for the smaller spheres, the MAP-MRF technique algorithm has a greater chance of recovering from this. The larger over-estimations returned for the smaller spheres with the EM technique, however, result in MAP-MRF results with large VOI errors.

To overcome the issue of over-estimation with the EM technique due to PVE, we introduce the spatial dependencies between the voxels at an earlier stage in the segmentation process, by applying the MAP-MRF EM technique. The introduction of a deconvolution pre-processing step is also applied. This de-blurring step takes into account  $B$  from (1), to provide a truer model of the real data, providing a clearer distinction between the 2 distributions present. Finally, we compare to previous results obtained using the FHMC approach.

Fig. 6 shows improvement for all the sphere VOIs returned with the MAP-MRF EM technique compared to the MAP-MRF technique. For all but 2 of the spheres, results returned also out-performed the T42 technique. We can see that the results of the MAP-MRF EM technique with the deconvolution pre-processing step provide the smallest volume errors in each case. Similar results were also found with this imagery for background ratios of 7.4:1 and 5.8:1. We then compare results to those previously obtained using a FHMC approach with 5 of the spheres, using the same type of phantom data with a signal to background ratio of 8:1 and an  $^{18}\text{F}$ -FDG concentration of 59.2kBq/ml in the spheres [2]. We can see that smaller volume errors are returned for the MAP-MRF EM technique with deconvolution for all but 1 sphere. In particular, we can see improved results for the smallest spheres, as no spatial correlation is lost with this method, unlike with the FHMC approach.

## 5. CONCLUSION

A MAP-MRF EM technique has been implemented to

provide VOI determination in PET. Results are promising, showing improvement over previous standard approaches. Computational complexity issues compared to the FHMC technique were compensated for by the use of convolution operations on 3D datasets. This resulted in execution times of less than 0.2 secs for each ICM iteration (using a 2800Mhz x86 GenuineIntel processor). The integrated approach applied also resulted in fast convergence. In general, for datasets of this size, the computational cost is not a major issue. We plan, however, to accelerate the algorithm further by offloading suitable parts to a Graphics Processing Unit, for parallel execution. Further work shall include the application of the technique to a greater range of datasets, including real PET imagery; and investigating the potential of updating the technique to take advantage of the Poisson distributed nature of raw PET data.

## 6. ACKNOWLEDGEMENTS

Funding was provided by Andor Technology, DEL NI and the NI HPSS R&D Office. PET datasets were provided by the NI Regional Medical Physics Agency.

## 7. REFERENCES

- [1] U. Nestle et al, "Comparison of different methods for delineation of 18F-FDG PET-positive tissue for target volume delineation in radiotherapy of patients with non-small cell lung cancer", *J Nucl Med*, 46, pp. 1342-1348, 2005.
- [2] M. Hatt et al, "Fuzzy Hidden Markov chains segmentation for volume determination and quantitation in PET", *Phys. Med. Biol*, 52, pp. 3467-3491, 2007.
- [3] J.L. Starck & E. Pantin, "Deconvolution in Astronomy: A Review," *Publications of the Astronomical Society of the Pacific*, 114, pp. 1051-1069, 2002.
- [4] X. Geets, J. A. Lee, A. Bol, & M. Lonnet, "A gradient-based method for segmenting FDG-PET images: methodology and validation", *Eur J Nucl Med Mol Imaging*, 34, pp. 1427-1438, 2007.
- [5] A. Dempster, N. Laird, & D. Rubin, "Maximum likelihood from incomplete data via the EM algorithm," *Journal of the Royal Statistical Society*, 39(1), pp. 1-38, 1977.
- [6] S. Z. Li, *Markov Random Field Modelling in Computer Vision*, New York: Springer-Verlag, 2001.
- [7] J. Besag, "On the statistical analysis of dirty pictures," *Journal of the Royal Statistical Society, Series B (Methodological)*, 48(3), pp. 259-302, 1996.
- [8] N.C. Krak et al, "Effects of ROI definition and reconstruction method on quantitative outcome and applicability in a response monitoring trial", *Eur J Nucl Med Mol Imaging*, 32, pp. 294-301, 2005.